THE QUEST FOR THE EQUATION OF STATE OF NUCLEAR MATTER IN THE ENERGY RANGE (0.1–2)*A* GeV*

W. Reisdorf

for FOPI Collaboration

Gesellschaft für Schwerionenforschung mbH
64291 Darmstadt, Germany

(Received December 11, 2001)

Heavy ion collisions in the energy region from $0.1A$ to $2A$ GeV are expected to yield information on the Nuclear Equation of State at baryon densities between roughly 1/3 and 3 times the saturation density of cold nuclei. Due to the complexities of heavy ion collision dynamics, the extraction of fundamental nuclear physics from the observables by comparisons with transport model simulations requires a rather complete and accurate systematics of data. Specifically, we discuss stopping and mixing, clusterization, pion production and the various manifestations of flow.

PACS numbers: 25.70.Pq, 25.75.+r

1. Introduction

The Equation of State (EoS) of nuclear matter, *i.e.* the relationship specifying how the pressure, or alternatively the energy per particle, depends on density and temperature, is of fundamental interest. It is relevant to astrophysical events and objects such as the Big Bang, supernovae explosions, and neutron stars.

Energetic heavy ion collisions are expected to yield information on the EoS. Indeed, when two heavy nuclei collide at sufficiently high energy they are compressed and heated up. A flow pattern will develop as the system subsequently expands. In macroscopic classical physics flow can be described in the language and with the tools of hydrodynamics [1, 2], where one links in a conceptually simple way conservation laws (mass, momentum, energy) with fundamental properties of the fluid: the equation of state and transport coefficients, such as viscosity and heat conductivity.

* Presented at the XXVII Mazurian Lakes School of Physics, Krzyże, Poland, September 2–9, 2001.

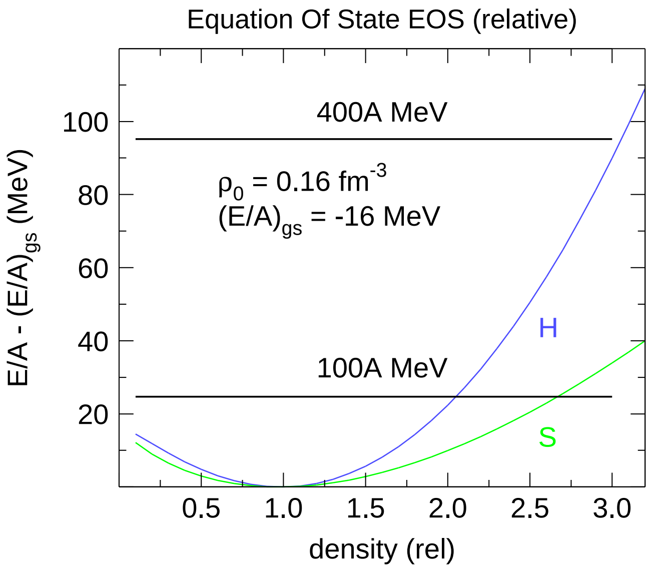

Fig. 1. Some typical 'hard' (H) and 'soft' equations of state used in the simulation of heavy ion collisions.

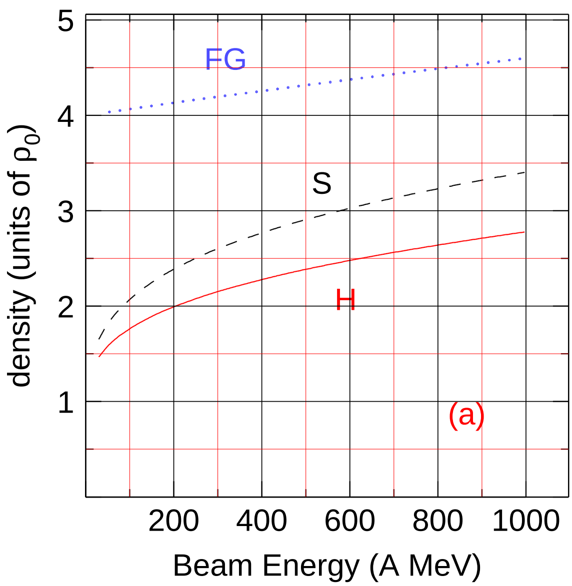

Fig. 2. Predicted maximum densities reached in heavy ion reactions (FG Fermi gas).

As the EoS is not known one compares the experimental observations with theoretical simulations using various assumed EoS, Fig. 1. The maximum density that can be reached can be very simply estimated from the Rankine–Hugoniot–Taub shock equations, Fig. 2. As we shall discuss in this presentation the simple link,

$$\text{experiment} \rightarrow \text{hydrodynamic simulation} \rightarrow \text{EoS},$$

has not materialized. In contrast to the assumptions of hydrodynamics the 'objects' we are trying to compress, the nuclei, are not macroscopically large, *i.e.* the surface/volume ratio is not negligible. Already for ground state masses (*i.e.* the EoS at zero temperature and saturation density $\rho_0 = 0.16\ \mathrm{fm}^{-3}$) the 'finite size' corrections (surface and Coulomb energy) to the bulk volume binding energy (-16 MeV) cut the effective binding energy per nucleon in half (-8 MeV). In heavy ion collisions the 'surface' is 3-dimensional because also the time is finite. As a consequence we have what I shall call the 'small object problem'. To infer nuclear properties from heavy ion data we must develop transport model codes which require in addition to the static EoS (mean field dependent on density), the dynamics of mean fields (momentum dependence) and copious information on the microscopic processes (nucleon–nucleon collisions and their modifications 'in the medium'). All this requires on the experimental side a large systematic effort delivering data of sufficient diversity and quality to constrain the many unknown parameters. This requires both in theory and experiment a monumental effort that is still going on.

Due to space limitation this presentation must be very incomplete. Complementary work is represented in this workshop by Danielewicz [3] (transport theory) and by Senger [4] (strangeness production).

2. Stopping and mixing

In the energy regime covered in this talk, $0.1A$ to $2A$ GeV, central heavy ion collisions will lead to the emission of about 60 particles at the low energy end and 200 particles at the high energy end. Such complex reactions are studied nowadays with use of large modular detector setups covering close to 4π sr. The FOPI detector is described elsewhere [5, 6]. Here we shall just mention that the apparatus consists of a large superconducting magnet providing a uniform solenoidal field of 0.6 T and housing two drift chambers for particle tracking. Highly granular scintillator arrays are arranged around and downstream of the drift chambers. Particle identification (by mass and charge) is generally based on the measurement of three quantities: the specific energy loss in the drift gas or in the scintillators, the magnetic rigidity (track curvature) and the time-of-flight (or velocity).

One of the basic questions to be answered first when studying heavy ion collisions is the following: are we anywhere close to the ideal hydrodynamic regime? The fast establishment of local equilibrium following complete stopping which is necessary to enter this regime, is governed by the mean free path $\lambda_{\rm free}$ of a nucleon in one of the ions in the 'medium' of the other ion which it is traversing. $\lambda_{\rm free}$ depends on the density reached and on the (known) elementary nucleon-nucleon cross sections σ_{nn}. The effect of varying the effective or 'in-medium' σ_{nn} is dramatic, as can be demonstrated in simulations using transport codes such as IQMD [7] based on quantum molecular dynamics [8]. Fig. 3 shows calculated invariant cross section contours in the plane of transverse momentum $p_t^{(0)}$ versus rapidity $y^{(0)}$ for central collisions of ^{96}Ru on ^{96}Ru at 400A MeV. Both $p_t^{(0)}$ and $y^{(0)}$ are given in scaled units, *i.e.* they are divided by the c.o.m. beam momentum and rapidity, respectively. Using half the known σ_{nn} values leads to a 'transparency' scenario, left panel. A 'hydro-shock', with nuclear matter ejected at 90°, is obtained if one uses $5 \times \sigma_{nn}$. Using $2 \times \sigma_{nn}$ does not lead to significant deviations from the hydro-shock topology, right panel in Fig. 3. Thus, deviations, downward or upward, by a mere factor two of the in-medium elementary cross sections are sufficient to proceed from 'gases passing thru each other' to 'droplets splashing on each other' [9, 10]. The projections of these topologies on the rapidity axis for protons and deuterons separately, are shown in Fig. 4 together with the measured data (circles), demonstrating that the experimental data are significantly different from both extreme scenarios. Specifically, to enter the hydrodynamic regime, we would have needed a system with twice the *linear* dimension of ^{96}Ru, or in three dimensions, eight times the mass, *i.e.* a collision of nuclei with masses $A = 800$! For the nominal σ_{nn} the IQMD calculation (solid curve) repro-

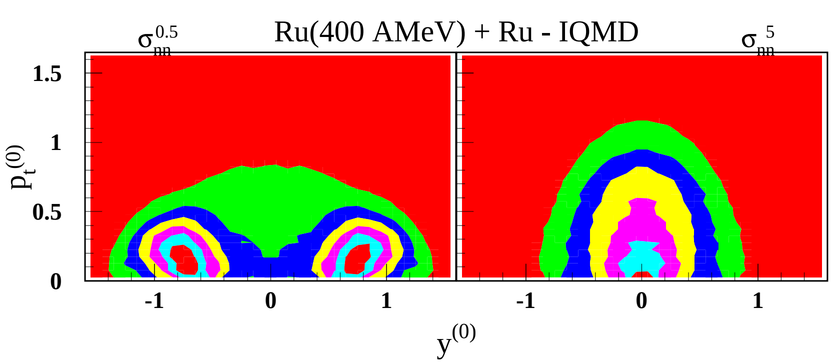

Fig. 3. Momentum space distributions in a transparency and a hydro-shock scenario.

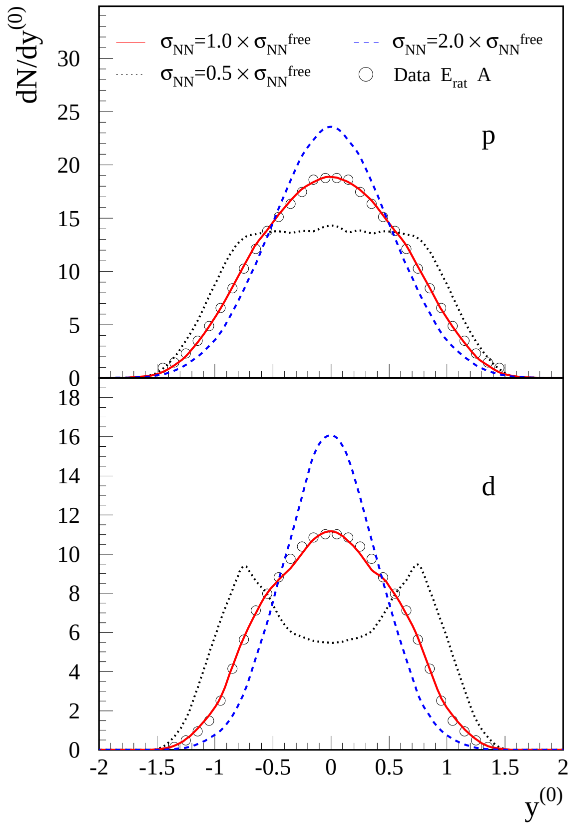

Fig. 4. Proton and deuteron rapidity distributions in the reaction ^{96}Ru+^{96}Ru at 400*A* MeV.

duces the data surprisingly well. It is important to realize that this *partial* transparency is in part a consequence of the fermionic nature of nucleons, which is approximated 'semi-classically' here by the Uehling–Uhlenbeck part of the collision term (Pauli blocking of the populated phase space).

Incomplete stopping in heavy ion collisions, evidenced by the present data by comparison with transport calculations, suggests that complete equilibration might not be reached. Such conclusions were reached more unambiguously (*i.e.* in principle without the need for transport calculations) by our Collaboration by using the isospin tracer method [11]. Here one studies systems such as ^{96}Ru+^{96}Zr that, while being symmetric in mass, are asymmetric in isospin. If one associates isospin to a 'colour' one can envision what might happen if two such differently coloured nuclei collide, Fig. 5. Provided one is not colour-blind, then for the transparent scenario one will observe the passing thru, while in the hydro-shock scenario a so-called 'rebound' is expected: the initially stopped and shocked material in the middle will cause additional incoming material to rebound on its borders. If one were to measure the neutron-to-proton ratio, N/Z, as a function of rapidity, one would expect specific slopes as shown in the figure.

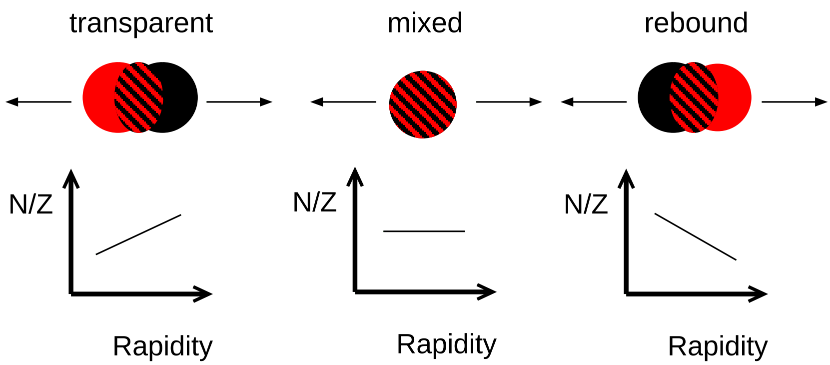

Fig. 5. Various scenarios in an isospin tracer experiment.

The actual experiment is based on a combined study of four systems: two symmetric ones, Zr + Zr and Ru + Ru, and two mixed systems, Zr + Ru and Ru + Zr (inverting projectile and target). The following observable was studied in Ref. [11]

$$R_Z = \frac{2N_y^{\mathrm{mix}} - N_y^{\mathrm{Zr}} - N_y^{\mathrm{Ru}}}{N_y^{\mathrm{Zr}} - N_y^{\mathrm{Ru}}}\,, \qquad (1)$$

where N_y^i is the differential yield at a given rapidity y for symmetric systems (Zr + Zr with i = Zr, Ru + Ru with i = Ru and the mixed systems Zr + Ru, respctively Zr + Ru with i = mix). This observable was designed to assess the differential rapidity distribution for proton-like (protons plus deuterons) ejectiles relative to that of the corresponding 'calibrating' symmetric systems. We also note in passing that the slope of R_z when varying rapidity is expected to be opposite to the schematic shown in Fig. 5. The result, together with IQMD simulations is shown in Fig. 6. Incomplete mixing is demonstrated by the fact that the data deviate from the horizontal line at $R_z = 0$. The 'standard' calculation (solid curve) reproduces the data well, the hydro-shock scenario, once more, is completely excluded (dotted curve with negative R_z).

The observation of partial transparency has dramatic consequences for the quest for the EoS, both theoretically and exprimentally. As we do not reach equilibrium, not even locally, we must use non-equilibrium theory with all its complications to link heavy ion data to 'simple', or 'fundamental' properties of hot and compressed nuclear matter. For transport codes it

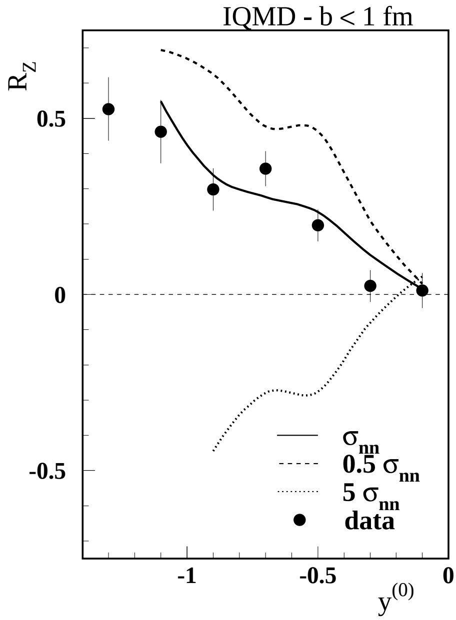

Fig. 6. Comparison of the proton counting observable with various IQMD simulations.

means that they have to be fed with momentum dependences of the mean fields (in addition to the density dependences) and with 'effective' cross sections for all the relevant microscopic processes, including possible in-medium modifications, a monumental task. The experiment must be able to provide as constraints complete and precise stopping power systematics as a function of incident energy, system size and ejected particle type, also a monumental task.

3. Expansion and clusterization

There is another observable that we must try to understand in more detail in this energy regime: the tendency of hot nuclear matter to be ejected in clusters, rather than as single nucleons. The fact that nucleons, which are fermions, coagulate to form nuclei is a fundamental nuclear physics fact that deserves our full attention also, and maybe especially, in the dynamic situation. As shown in Fig. 7, the probability for a proton to appear attached to at least one other nucleon decreases rather slowly from about 80% at $200A$ MeV to still 50% at $1A$ GeV. As in these energies the 'available' c.o.m. energies are well beyond typical nucleon binding energies, dynamic mechanisms, such as cooling by adiabatic expansion, or non-equilibrium processes

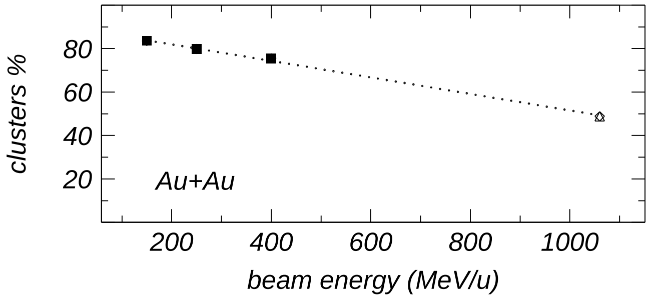

Fig. 7. Degree of clusterization (%) of protons in central Au on Au collisions.

must be invoked to explain such high degrees of clusterization. Indeed, attempts to parameterize the observed cluster size distributions, which are exponential functions in central collisions, in terms of thermal 'freeze-out' models lead to very low apparent temperatures as is shown in Fig. 8. Taken at face value the thermal part of the available energy would represent only about 20%, leaving us with the difficult task of identifying 80% of the energy as collective 'flow'.

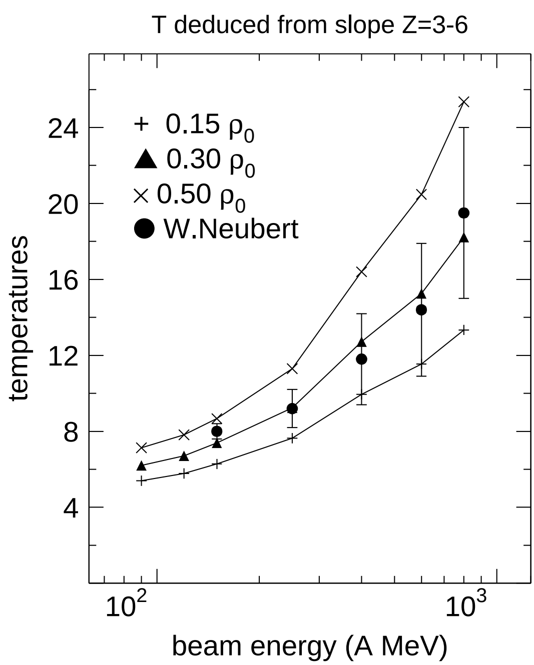

Fig. 8. Apparent 'temperatures' deduced from the cluster distributions in central collisions as a function of the beam energy.

An alternative interpretation of the cluster data is in terms of a non-equilibrium process specific to fast expansion dynamics and first suggested by Grady *et al.* [12] to account, in a very different context, for the distribution of clusters of galaxies (following also an exponential decrease) in a 'slightly' bigger system: the expanding Universe. The idea [12] is that in a flow field strong *gradients* of flow, rather than 'temperatures', determine how preformed clusters of nucleons manage to stick together, just when expanding below the saturation density. In Fig. 9 we demonstrate that the average fragment size seems to be linearly correlated with the inverse of the radial flow. In two-particle correlation studies (which yield information related to that of cluster formation probability) similar mechanisms determine the deduced apparent radii: they are governed by the size of regions of homogeneity (within which flow gradients are modest). Such ideas are supported by recent simulations [13].

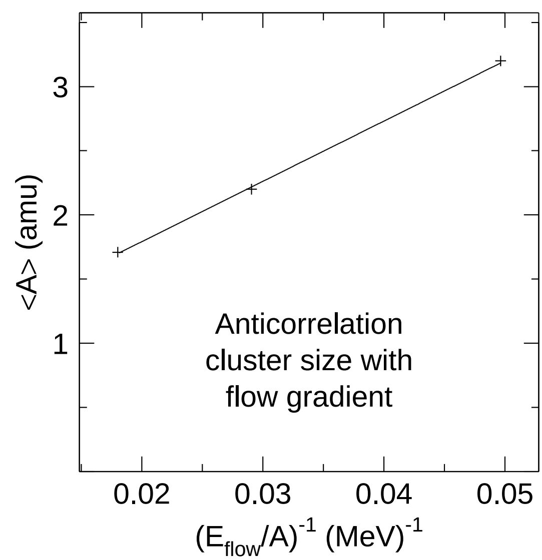

Fig. 9. Variation of the average cluster-size with the inverse radial flow.

As is the case also for other observables (to be discussed below), further complications arise from the 'small object problem'. Cluster formation probabilities are found experimentally to be system-size dependent, see Fig. 10. We have varied the system size from Ca + Ca ($Z_{\rm proj} = 20$) all the way to Au + Au ($Z_{\rm proj} = 79$). Even if we take out the trivial size dependence (relative to Au) by scaling the multiplicities with $Z_{\rm Au}/Z_{\rm proj}$, we observe significantly higher Li fragment multiplicities in the larger systems, with no obvious tendency to 'saturate' at the heavy end. Again, this weakens interpretations in terms of global thermal models and points to rather large

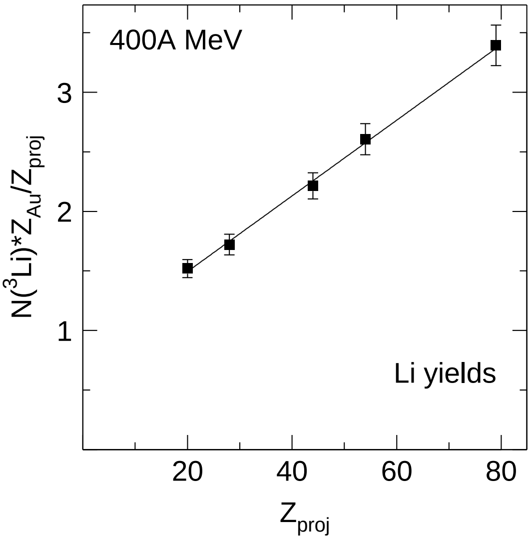

Fig. 10. System size dependence of Li cluster multiplicities in central collisions at 400A MeV.

surface to volume ratio effects. Correlations of this observable with stopping power, expansive flow, *etc.*, are under investigation. We expect interesting clues also about the vapour to liquid transition from such studies.

4. The rise and fall of flow

The term 'flow' is borrowed from hydrodynamics. One treats the motion of many fluid cells, each one containing many atoms or molecules (nucleons or hadrons in our context) moving with a collective cell velocity 'flow', while inside the cell a disordered (maybe 'locally' thermalized) motion takes place. On the absolute scale, radial expansion due to the action of pressure gradients has the largest 'flow' components. It is however easier to observe and define azimuthal asymmetries in the particle emission patterns, that occur in non-central collisions and are based on the existence of an observable reaction plane serving as reference for the third-dimension coordinate, the azimuth ϕ (in addition to p_t and the rapidity). We start by defining a scaled global measure of the so-called directed sideflow $p_x^{\rm dir}$

$$\begin{aligned} p_x^{\rm dir} &= \frac{\sum_i \mathrm{sign}\,(y_i) Z_i u_{xi}}{\sum_i Z_i}\,, \\ u_{xi} &= \frac{\vec{u}_{ti}\cdot\vec{Q}_i}{|Q_i|}\,, \end{aligned}$$

$$\vec{Q}_i = \sum_{j \neq i} Z_j \vec{u}_{tj} \,, \qquad \vec{u} = \frac{\vec{\beta}\gamma}{\beta_p \gamma_p} \,.$$

The sum for $p_x^{\rm dir}$ extends over all observed charged (Z_i) particles with scaled four-velocities u (u_t being the transverse component). The reaction plane vector $\vec{Q}_i$ [14] used for the definition of the in-plane component u_{xi} does not include the particle i to avoid autocorrelations.

When defining the reduced impact parameter $\hat{b} = b/b_{\rm max}$, where $b_{\rm max} = 1.15(A_p^{1/3} + A_t^{1/3})$, with A_p and A_t the projectile and target masses, one finds that the directed sideflow peaks around $\hat{b} = 0.35 \pm 0.05$. Impact parameter sorting is generally done by using sharp-cut geometric interpretations of the measured distribution of global event observables, such as total particle multiplicities or ERAT-the ratio of total transverse to longitudinal kinetic energy [15].

In Fig. 11 we follow directed sideflow near $\hat{b} = 0.35$ for Au + Au as a function of incident energy from $90A$ MeV to $1500A$ MeV. We observe a remarkable rise and fall of scaled sideflow in this energy regime, with a maximum of 16% (in units of the c.o.m. beam momentum) near $400A$ MeV. We recall that ideal-gas non-viscous hydrodynamics would predict a perfectly flat excitation function. The observed characteristic shape of the excitation function calls for a search for other correlated observables in order to find experimental clues to the mechanisms behind the sideflow phenomenon.

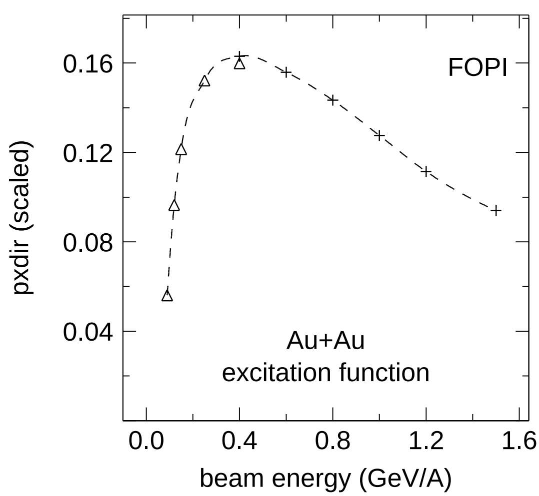

Fig. 11. Excitation function of sideflow in Au on Au collisions.

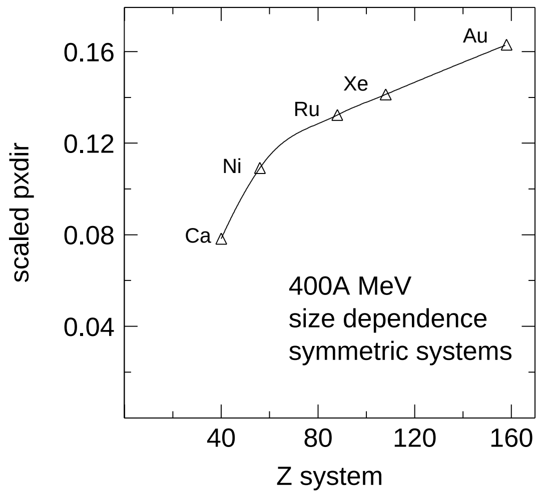

Fig. 12. System size dependence of sideflow at $400A$ MeV.

Another important piece of information is the observed system-size dependence of sideflow for symmetric systems shown for $400A$ MeV beam energy in Fig. 12. Again, we are faced with the small-system consequences. It is remarkable that sideflow does not show any tendency to 'saturate' even for the heaviest system (Au+Au). This has to be seen in conjunction with the stopping studies just discussed, where we concluded that the ideal hydrodynamic limit would require (unavailable) projectiles much heavier than Au. Sideflow does not only depend on the stiffness of the EoS, but is also influenced by the stopping power. Partial transparency simulates a soft EoS and *must* therefore be accounted for realistically in transport calculations.

4.1. Spectators as a clock

Concerning the fast rise [16] of scaled sideflow in the energy range between $90A$ and $250A$ MeV, it is tempting to correlate it with the onset of compression and of radial flow. Above $100A$ MeV, *scaled* radial flow [15] does not vary in any significant way however. Very recent measurements by the INDRA collaboration [17] show that radial flow in Au on Au collisions sets in just above $30A$ MeV and reaches scaled values comparable to those at $400A$ MeV already at $100A$ MeV. If one envisions sideflow as resulting from fireball matter exploding into spectator matter, one wonders why sideflow does not follow exactly the behavior of radial flow. A qualitative clue is given in Fig. 13 which shows momentum space topologies for Li fragments in Au on Au collisions at 90, 150 and $400A$ MeV for the same centrality, $\hat{b} = 0.35$ (in the maximum of sideflow). The most conspicuous feature is the increasing separation of 'spectator' sources as the energy is raised. At

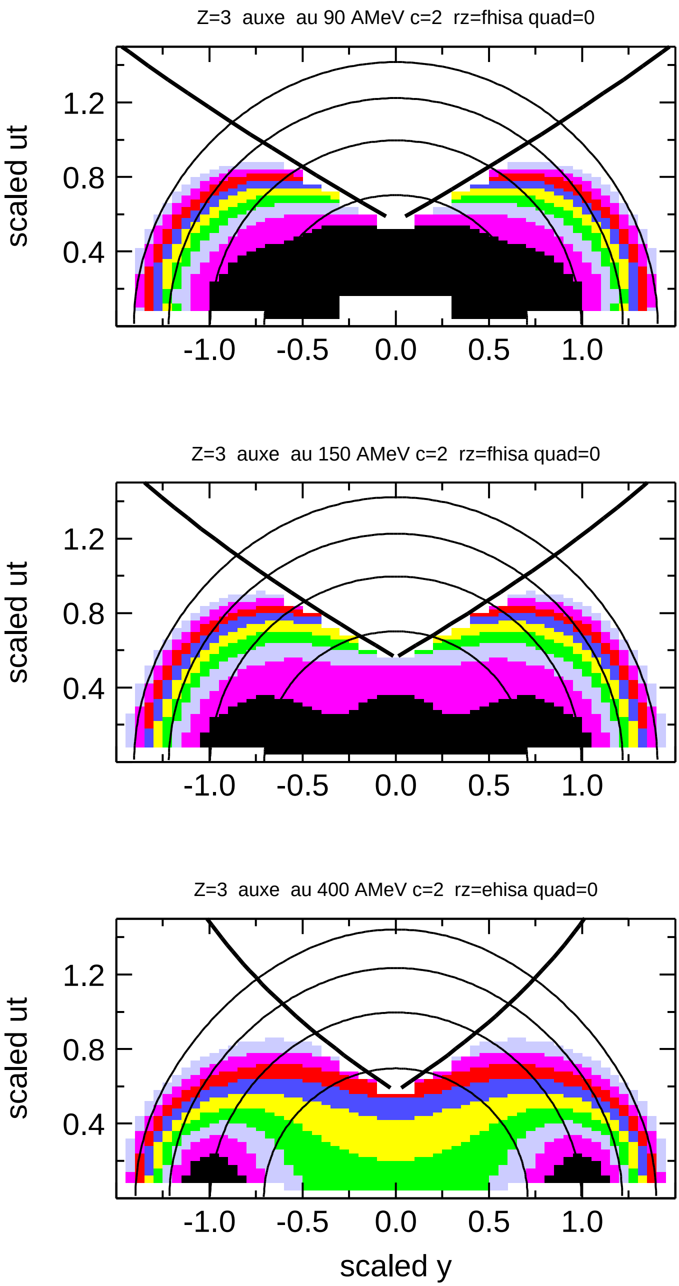

Fig. 13. Momentum space topologies of Li fragments in Au+Au collisions at 90, 150, 400A MeV (top to bottom) for $\hat{b} \approx 0.35$

the lower energy there is more time for spectators and participants to mix due to Fermi motion: *this weakens the sideflow.* Indeed one has to compare the passing time ($2R/u$) (R projectile radius, u four-velocity) which varies from about 60 fm/c (90A MeV) to about 30 fm/c (400A MeV) with the Fermi-time of about 60 fm/c (typical time for a nucleon to cross the system due to its Fermi motion).

4.2. The rise of nucleonic excitations

In the energy range from 400 to 1500A MeV, sideflow (Fig. 11) is decreasing by a factor 1.7. Among the causes that are invoked for this phenomenon are the decreasing passing time, the increase of transparency, the decrease of the momentum dependent repulsion, and, of course the softening of the EoS. The passing time is decreasing by a factor 1.9. Roughly speaking, final (observed) flow results from the product of the pressure gradient (which has a mean field and a kinetic component) with the passing time. A decreasing flow due only to a decreasing (spectator) passing time would imply that the pressure gradient does not increase significantly with increasing energy.

What is changing in this regime is the gradual rise of the probability of exciting internal degrees of freedom of the nucleon, which deexcite primarily by pion emission, degrees of freedom that are still frozen below 400A MeV.

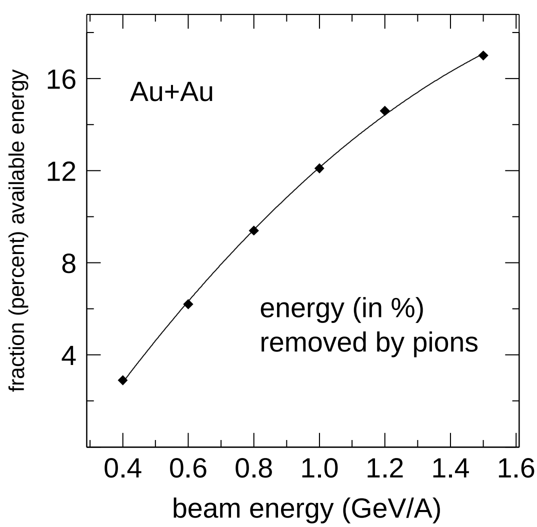

Fig. 14. Fraction of the available energy removed by pions in central collisions of Au on Au as a function of the beam energy.

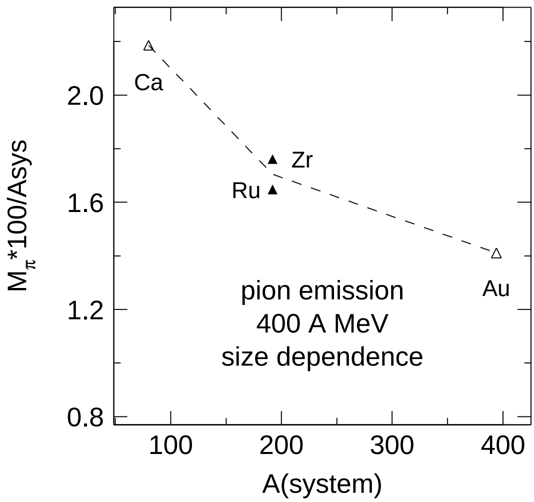

Fig. 15. System size dependence of pion multiplicities at 400A MeV.

Figure 14 shows the measured rise of the fraction of energy removed by pion creation and emission. One could argue that this energy is not available for sideflow generation. A rough estimate shows however that this does *not* quantitatively account for the decrease of sideflow. On the contrary, one might expect that the pion wind hitting the spectators will accelerate the latter, causing sideflow. Clearly pion creation must increase the stopping power. The actual cause for the decrease of sideflow still requires further investigation. As with all other observables, pion emission per nucleon in central collisions shows also pronounced surface/volume effects (as well as isospin effects) as shown in Fig. 15. The shown pion data are still preliminary.

5. Elliptic flow and the EoS

Flow is one of the prime observables (for the 'Kaon observable' see [4]) expected to constrain our ideas about the EoS. For space reasons we shall discuss this aspect here only for the so called elliptic flow, stressing that a convincing transport theory code must also reproduce the other manifestations of flow and the other observables, such as stopping, degree of clusterization (entropy) and pion emission characteristics discussed earlier.

In modern data analysis that studies momentum space population in full three-dimensional glory, it is customary to Fourier analyse the azimuthal distributions. Finite reaction plane resolution problems (with typically 20°

to 30° azimuthal uncertainty) limit such expansion to

$$E\frac{dN}{d^3p} = \frac{1}{\pi}\frac{d^3N}{dp_t^2dy}(1 + 2v_1 \cos\phi + 2v_2 \cos 2\phi)\,.$$

The Fourier coefficient $v_1 = \langle\cos\phi\rangle = \langle p_x/p_t\rangle$ (the component x is in-plane perpendicular to the beam axis z) is associated to the directed sideflow. The coefficient $v_2 = \langle\cos(2\phi)\rangle = \langle(p_x/p_t)^2 - (p_y/p_t)^2\rangle$ is called 'elliptic' flow and corresponds for negative values to preferential out-of-plane emission ('squeeze-out'). An alternative for v_2 is the ratio $R_N = (1-2v_2)/(1+2v_2)$ of the 90°/0° emission probability. One finds both v_1 and v_2 to be p_t and y (rapidity) dependent implying a wealth of information.

We have studied elliptic flow in two separate experiments. The results (in terms of v_2) for the 'high' energy experiment (from 400 to 1500A MeV), which are still preliminary [18], are shown in Fig. 16, the data for the 'low' energy experiment (in terms of R_N [19]) are shown in Fig. 17 together with transport calculations demonstrating the sensitivity to the EoS and the problems connected with such comparisons. Above about 200A MeV the calculations show sensitivity to the mean field: in Fig. 16 the prediction without mean field is labelled 'cascade', calculations [20] with a soft, or hard, momentum dependent EoS (compressibility $K = 220$, or 379 MeV), are labelled SM, or HM. Clearly the data (full symbols) exclude the cascade option, but

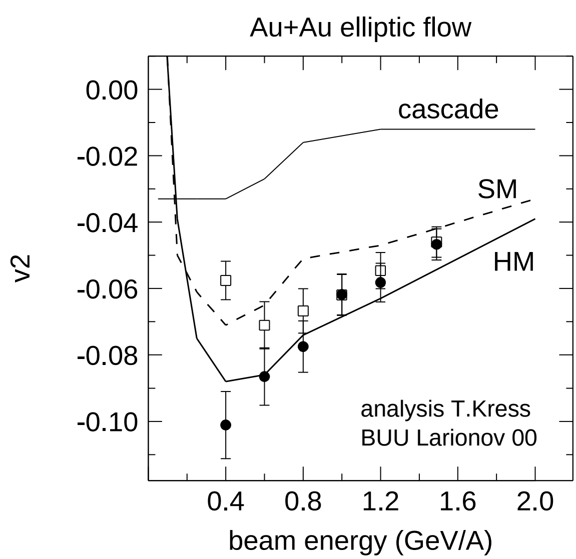

Fig. 16. Comparison of measured elliptic flow with simulations assuming various EoS.

seem to suggest a gradual transition from 'hard' to 'soft' (suggested possibly also by the sideflow observable, Fig. 11). We note that below 600A MeV the contribution from clusters (included in the data) is important as can be inferred by comparing to data for single protons (open symbols). In

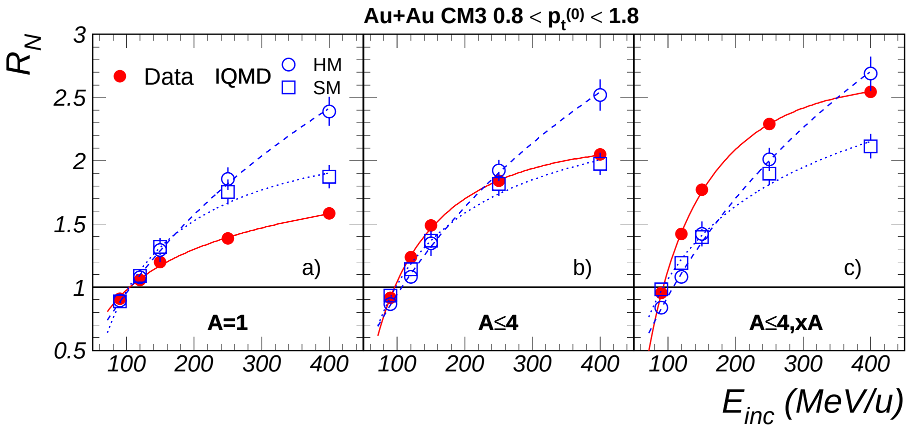

Fig. 17. Excitation function for the squeeze-out signal in mid-central reactions of Au on Au together with IQMD model predictions.

the low energy regime clusters become essential. In Fig. 17 the left panel shows the excitation function of elliptic flow for protons, the middle panel for all ejectiles with mass number up to 4 added linearly with equal weights, and in the right panel the addition is weighted with the mass number ('coalescence invariant'). The conclusions that one would be tempted to draw from comparisons with the IQMD transport code are dramatically different for the three excitation functions. While the single proton flow is overestimated by both the SM and HM calculations (left panel), it is evident for the 'coalescent invariant flow' (right panel) that the shape of the excitation function is not understood. It is too early to draw definite conclusions. We note that IQMD strongly underestimates cluster formation.

6. Conclusion

The quest to obtain constraints on the nuclear EoS by confronting transport model simulations with heavy ion collision data is still ongoing. Flow data (and also sub-threshold kaon production data [4]) show sensitivity to the EoS. To support the uniqueness and the credibility of the conclusions, much further work is necessary. Transport model calculations are convincing only if they have *all* observables 'under control'. This implies reproducing stopping and mixing data, the chemistry of the out-freezing fireball, in-medium particle production dynamics and the full 3-dimensional topology of the observed momentum space populations. All observables have a pronounced system size dependences which must also be understood.

REFERENCES

[1] H. Stöcker, W. Greiner, *Phys. Rep.* **137**, 277 (1986).
[2] R.B. Clare, D. Strottman, *Phys. Rep.* **141**, 177 (1986).
[3] P. Danielewicz, *Acta Phys. Pol.* **B33**, 20 (2002).
[4] P. Senger, *Acta Phys. Pol.* **B33**, 125 (2002).
[5] A. Gobbi *et al.*, *Nucl. Instrum. Methods Phys. Res.* **A324**, 156 (1993).
[6] J. Ritman, *Nucl. Phys. B Proc. Suppl.* **B44**, 708 (1995).
[7] C. Hartnack *et al.*, *Eur. Phys. J.* **A1**, 151 (1998).
[8] J. Aichelin, *Phys. Rep.* **202**, 233 (1991).
[9] G.J. Bertsch, *Phys. Rev. Lett.* **34**, 697 (1975).
[10] W. Scheid, H. Müller, W. Greiner, *Phys. Rev. Lett.* **32**, 741 (1974).
[11] F. Rami *et al.*, *Phys. Rev. Lett.* **84**, 1120 (2000).
[12] B.L. Holian, D.E. Grady, *Phys. Rev. Lett.* **60**, 1355 (1988).
[13] S. Chikazumi *et al.*, *Phys. Lett.* **B476**, 273 (2000).
[14] P. Danielewicz, G. Odyniec, *Phys. Lett.* **B157**, 146 (1985).
[15] W. Reisdorf *et al.*, *Nucl. Phys.* **A612**, 493 (1997).
[16] F. Rami *et al.*, *Nucl. Phys.* **A646**, 367 (1999).
[17] F. Lavaud, thesis, 2001, U. Strasbourg.
[18] T. Kress (FOPI Collaboration), priv. communication.
[19] A. Andronic *et al.*, *Nucl. Phys.* **A679**, 765 (2001).
[20] A.B. Larionov *et al.*, *Phys. Rev.* **C62**, 064611 (2000).